Shock waves in strongly interacting Fermi gas from time-dependent density functional calculations

F. Ancilotto,[1,2] L. Salasnich,[1] and F. Toigo[1,2]

[1]*Dipartimento di Fisica e Astronomia "Galileo Galilei" and CNISM, Università di Padova, Via Marzolo 8, 35122 Padova, Italy*

[2]*CNR-IOM Democritos, via Bonomea, 265-34136 Trieste, Italy*

(Received 16 April 2012; published 13 June 2012)

Motivated by a recent experiment [Phys. Rev. Lett. **106**, 150401 (2011)], we simulate the collision between two clouds of cold Fermi gas at unitarity conditions by using an extended Thomas-Fermi density functional. At variance with the current interpretation of the experiments, where the role of viscosity is emphasized, we find that a quantitative agreement with the experimental observation of the dynamics of the cloud collisions is obtained within our superfluid effective hydrodynamics approach, where density variations during the collision are controlled by a purely dispersive quantum gradient term. We also suggest different initial conditions where dispersive density ripples can be detected with the available experimental spatial resolution.

DOI: 10.1103/PhysRevA.85.063612 PACS number(s): 67.85.−d, 03.75.Ss, 05.30.Fk

A Fermi gas of atoms at unitary conditions, i.e., when the *s*-wave scattering length diverges [1], is predicted to obey universal hydrodynamics, where the shear viscosity and other transport coefficients are universal functions of density and temperature. Experiments on the expansion of rotating, strongly interacting Fermi gas in the normal fluid regime reveal extremely low viscosity hydrodynamics [2], thus making a strongly interacting Fermi gas in the normal fluid regime a nearly perfect fluid with almost frictionless mass flow. Remarkably, the superfluid behaves in rotating cloud experiments almost identical to the normal fluid one. Consistent with such observations, theory predicts [3] that the unitary Fermi gas has zero bulk viscosity in the normal phase, whereas in the superfluid phase two of the three bulk viscosities vanish [4,5].

Nonlinear evolution of trapped cold gases is often characterized by the appearance of wavelike localized distortion of the trapped gas cloud. In addition to the well-known sound waves, shock waves often appear, which are characterized by an abrupt change in the density of the medium [6,7]. Shock waves are ubiquitous and have been studied in many different physical systems [6,7]. Very recently the observation of nonlinear hydrodynamic waves has been reported in the collision between two strongly interacting Fermi gas clouds of ^{6}Li atoms at unitarity [8]. During the collision, which has been experimentally imaged in real time [8], when regions of high density move with faster local velocity than regions of low density, large density gradients develop when the two clouds merge with each other. Unlike the case of collision between two initially separated BEC in a cigar-shaped trap, where the shock waves were interpreted as purely dispersive [9], the authors of Ref. [8] invoke dissipative forces to avoid the "gradient catastrophe" in the unitary Fermi system. To describe their experimental data, they use an effective one-dimensional (1D) model based on time-dependent nonlinear hydrodynamical equations, with a phenomenological kinematic viscosity term added to describe dissipative effects, whose strength is used as a fitting parameter. A quite high value of the viscosity coefficient is necessary in the description of the collision in order to reproduce the experimental data. The origin of such viscosity, however, is not clarified in Ref. [8]. In fact the role of dissipation itself in cold Fermi gas at low temperature is questionable, since the ultracold unitary Fermi gas is known as an example of an almost perfect fluid, as discussed above. In this paper we offer an alternative explanation, where the collision process is dominated by dispersion effects [10]. Evidence supporting the notion that shock waves in ultracold Fermi gas at unitarity are dispersive rather than dissipative can be found in the simulations reported in Ref. [11], based on the self-consistent solution of coupled Bogoliubov–de Gennes (BdG) equations derived from the zero-temperature time-dependent superfluid local density approximation [12]. Our calculations are based on a single-orbital density functional (DF) approach to the properties of unitary Fermi gas at low temperatures, which has been used recently to successfully address a number of properties of such a system [13–18]. The advantage in using a single-orbital DF approach is that systems with a very large number of particles can be treated using only a single function of the coordinate, i.e. the particle density. Thus, it might represent a viable alternative to the much more computationally expensive approaches (like, e.g., the Bogoliubov–de Gennes method) often used to describe superfluid Fermions. This is especially true in the case of 3D geometries, like the ones investigated here, where the BdG method would be prohibitively costly.

In our extended Thomas-Fermi (ETF) density functional approach [13,14] the total energy of the unitary Fermi gas is given by

$$E[n] = \int d^3\mathbf{r}\, \mathcal{E}(n, \nabla n), \tag{1}$$

where

$$\mathcal{E}(n, \nabla n) = \lambda \frac{\hbar^2}{8m} \frac{(\nabla n)^2}{n} + \xi \frac{3}{5} \frac{\hbar^2}{2m} (3\pi^2)^{5/3} n^{5/3} + U(\mathbf{r})\, n\ . \tag{2}$$

Here $n(\mathbf{r})$ is the fermion number density and $U(\mathbf{r})$ is the confining external potential. The total energy functional $\mathcal{E}$ contains a term proportional to the kinetic energy of a uniform noninteracting fermion gas, plus a gradient correction of the von Weizsacker form [19]. In recent papers [13–15,17], we have determined the parameters ξ and λ by fitting Monte Carlo results [20,21] for the energy of fermions confined in a spherical harmonic trap close to unitary conditions. The main

 ©2012 American Physical Society

conclusion of that work is that the values

$$\xi = 0.40 \quad \text{and} \quad \lambda = 1/4 \tag{3}$$

fit quite well Monte Carlo data of the unitary Fermi gas. In particular the chosen value for ξ almost coincides with the experimental determination of Ref. [22].

The density functional (1) describes various static and dynamical properties of the unitary Fermi gas trapped by an external potential. The gradient term in the previous equation is found to be crucial to describe accurately the surface effects of the system, in particular in systems with a small number of atoms, where the Thomas-Fermi (local density) approximation fails [13,15]. As a key result of the present paper, we show that when fast dynamical processes occur and/or when shock waves come into play, such a term is necessary also in the large-N limit.

The extended nonviscous and irrotational hydrodynamics equations deriving from the functional (1) are given by

$$\frac{\partial n}{\partial t} + \nabla \cdot (n\mathbf{v}) = 0 \,, \tag{4}$$

$$m\frac{\partial \mathbf{v}}{\partial t} + \nabla\left(\frac{m}{2}v^2 + \frac{\partial \mathcal{E}}{\partial n} - \nabla \cdot \frac{\partial \mathcal{E}}{\partial(\nabla n)}\right) = \mathbf{0} \,, \tag{5}$$

where $n(\mathbf{r},t)$ is the time-dependent scalar density field and $\mathbf{v}(\mathbf{r},t)$ the time-dependent vector velocity field. If $\lambda = 0$, then Eqs. (4) and (5) reproduce the equations of superfluid hydrodynamics [23] by construction.

Notice that Eqs. (4) and (5) can equivalently be written in terms of a superfluid time-dependent nonlinear Schrödinger equation (NLSE) involving a complex order parameter [13]. We will numerically solve this NLSE equation to obtain the long-time dynamics of the collision between two initially separated Fermi clouds, as described in the following. Our goal is to simulate the experiments of Ref. [8]. We have used the Runge-Kutta-Gill fourth-order method [24] to propagate in time the solutions of the NLSE. To accurately compute the spatial derivatives appearing in the NLSE, we used a 13-point finite-difference formula [25].

Since the confining potential used in the experiments is cigar-shaped, we have exploited the resulting cylindrical symmetry of the system by representing the solution of our NLSE on a two-dimensional (r,z) grid (of 500×2500 uniformly spaced points). Of course, this choice, which greatly reduces the computational cost of the simulations, would not be able to describe possible, azimuthal-dependent, transverse instabilities and vortex formation (like those observed in the collision between BEC clouds [9]). Although such features are apparently not observed in the collision experiments of Ref. [8], we cannot rule out the possibility of transverse instabilities and vortex formation in Fermi gas clouds for different initial conditions than those investigated here. To describe the details of such structures, a full 3D simulation is needed.

In our simulations we tried to reproduce as closely as possible the experimental conditions of Ref. [8], which we summarize briefly in the following. A 50:50 mixture of the two lowest hyperfine states of ^{6}Li is confined by an axially symmetric cigar-shaped laser trap, elongated along the z axis. The resulting trapping potential is $U(r,z) = 0.5m[\omega_r^2 r^2 + \omega_z^2 z^2]$, with $\omega_r = 2\pi \times 437$ Hz and $\omega_z = 2\pi \times 27.7$ Hz. The trapped Fermi cloud is initially bisected by a blue-detuned beam that provides a repulsive knife-shaped potential. This potential is then suddenly removed, allowing the two separated parts of the cloud to collide with each other. The system is allowed to evolve for a given hold time t, then the trap is removed in the radial direction, and the system is allowed to evolve for another 1.5 ms during which the gas expands in the r direction (during this extra expansion time, the confining trap frequency along the z axis is changed to $\omega_z = 2\pi \times 20.4$ Hz), and finally a (destructive) image of the cloud is taken. The process is repeated from the beginning for another different value for the hold time t. The experimental results are eventually plotted as 1D integrated density profiles for the different hold times investigated: In Fig. 2 of Ref. [8], the experimental 1D density profiles at different times t are shown along the long trap axis.

We simulated the whole procedure within the framework discussed above. As in Ref. [8], we chose the initial density profile in the form of a static solution of hydrodynamic equations:

$$n(r,z,t=0) = \tilde{n}\left(1 - \frac{r^2}{R^2} - \frac{z^2}{R_z^2} - \frac{V_{\rm rep}(z)}{\mu_G}\right)^{3/2} , \tag{6}$$

where $\tilde{n} = [(2m\mu_G/\hbar^2)/\xi]^{3/2}/(3\pi^2)$. $V_{\rm rep}$ represents an optically generated knife-shaped repulsive potential used to initially split the Fermi cloud into two spatially separated components that are led to collide with each other upon removal of such potential. $V_{\rm rep} = V_0 \exp[-(z-z_0)^2/\sigma_z^2]$, where $V_0 = 12.7\,\mu$K, $\sigma_z = 21.1\,\mu$m, and $z_0 = 5\,\mu$m. In Eq. (6) we use the same values as in Ref. [8], which provide a fit to the observed initial experimental cloud density profile immediately after the removal of the knife potential. Here $R_z = 220\,\mu$m and $R = 14\ \mu$m. In particular, the chosen value for the chemical potential $\mu_G = 0.53\ \mu$K corresponds to a total of $N = 2 \times 10^5$ ^{6}Li atoms.

During the time evolution of our system, when the two clouds start to overlap, many ripples whose wavelength is comparable to the interparticle distance are produced in the region of overlapping densities. These ripples also propagate backward toward the trap boundaries, affecting a larger and larger portion of the simulated cloud. We stress that these effects are quite similar to those found in a recent experiment [9] by merging and splitting Bose-Einstein condensates.

In order to properly compare our results with the experimental data of resonant fermions [8], which are characterized by a finite spatial resolution, we smooth the calculated profiles at each time t by local averaging the density within a space window of $\pm 5\ \mu$m centered around the calculated point. This procedure will give smoothed density profiles with a spatial resolution close to the one characterizing the experimental setup of Ref. [8].

The effect of smoothing is shown in Fig. 1, where the simulated density profile during the time evolution of the colliding clouds is shown before and after the local averaging procedure is applied. We wish to stress that this smoothing procedure is just a postprocessing of the data obtained by the time evolution of the NLSE corresponding to Eqs. (4) and (5), and therefore it does not affect the time evolution itself.

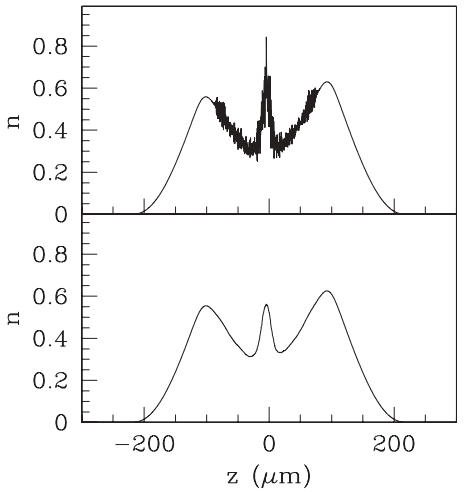

FIG. 1. Density profile after $t = 1.5$ ms. The two curves show the smoothed and nonsmoothed calculated profiles, respectively. The normalized density is in units of $10^{-2}/\mu$m per particle.

The results of our simulations (solid lines), for the whole time duration of the experiments, and after the smoothing procedure is applied to the (y-averaged) density profile at each time, are shown in Fig. 2 plotted along the long trap axis, for the same time frames as in the experiment. The experimental results (dotted lines) are also shown for comparison.

The time value shown in each frame corresponds to the time evolution of the initial profile, Eq. (6), before the trap in the radial direction is removed to let the system evolve for another 1.5 ms in the axial trap only, as done in the experiment.

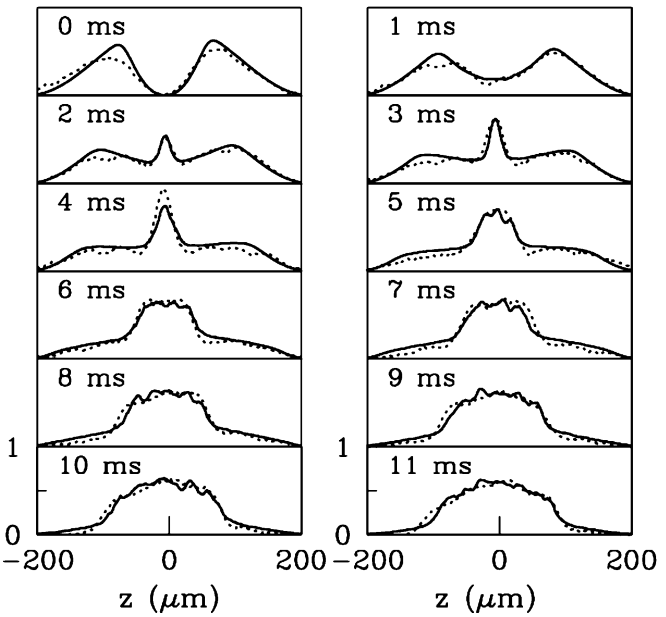

FIG. 2. 1D density profiles at different times t showing the collision of two strongly interacting Fermi clouds. Solid lines: our calculations with no adjustable parameter. Dotted lines: experimental data from Ref. [8]. The normalized density is in units of $10^{-2}/\mu$m per particle.

Note the striking correspondence between the experimental data and our simulation. We emphasize the fact that our simulations do not have an adjustable parameter to be used to fit the experimental data, at variance with the model calculations presented in Ref. [8]. Even after the smoothing procedures is applied, our simulated density profiles exibit short-scale structures superimposed to the body of the cloud profiles. Such ripples are indeed present also in the experimental data, whereas in the model profiles used in Ref. [8] to fit the observed images such oscillations are completely absent, due to the presence of a strong viscosity term in their model.

The numerical results shown in Fig. 2 have been obtained by using $\lambda = 1/4$, as previously discussed. In order to check the dependence of our results against a different choice for λ, we have performed various time-dependent calculations with the same initial conditions but using different values for λ. It turned out that changing λ from the optimal value $\lambda = 1/4$ has profound consequences on the long-time evolution of the colliding clouds, providing density profiles that are completely different from the experimental ones.

This finding is not simply a numerical result, but has an important physical bearing. In fact, a strong dependence on λ of the time evolution of a Fermi cloud made of a large number of atoms is at first sight surprising, given the fact that the gradient term should become less and less important with increasing N. We believe that such dependence is due to the presence of shock waves (i.e., regions characterized by large density gradients) in the colliding clouds. To check this hypothesis one should perform experiments with different initial conditions, which do not evolve into shock waves. As an example, we have simulated a "soft" collision, where shock waves are not expected, by considering a system with a smaller density of fermions ($N = 4000$ in the same trap used in the simulations of Fig. 2) and where the two initial clouds are largely overlapping at the beginning of the simulation (this

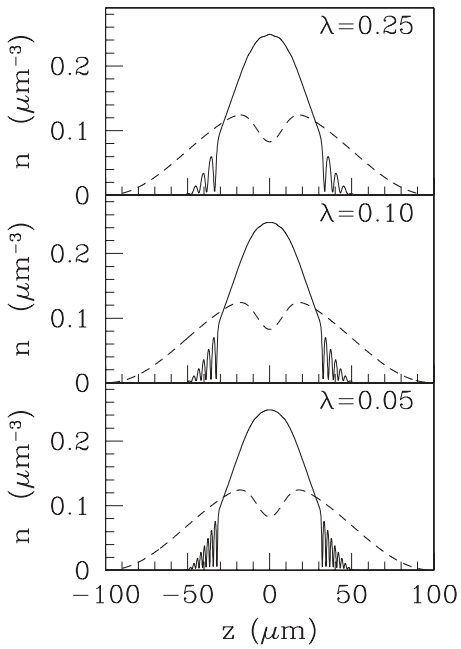

FIG. 3. "Soft" collision. The initial density profile is shown with dashed lines.

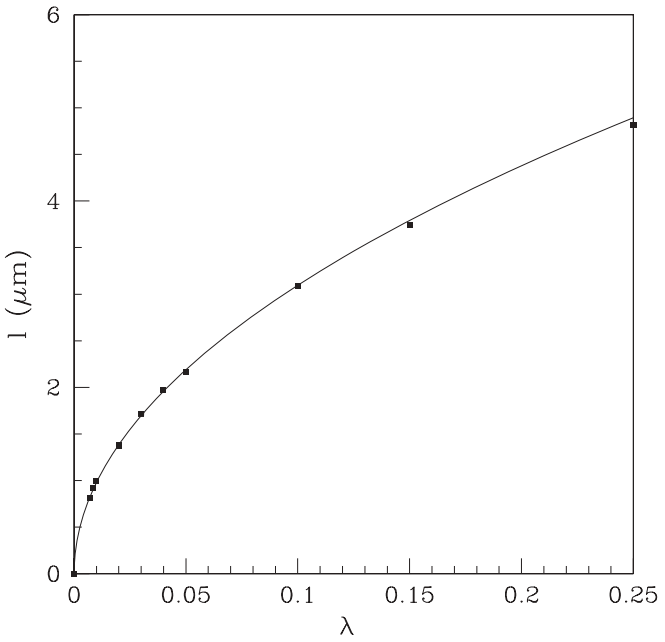

FIG. 4. Ripple wavelength l as a function of gradient coefficient λ of the density functional. The solid line shows the $\sqrt{\lambda}$.

could be obtained experimentally by reducing the height or width of the "knife potential"), thus reducing the velocity of the impinging clouds. It turns out that the long-time behavior of such a system is indeed *independent* from the chosen value of λ. However, even for such a system, shock waves will eventually occur. As expected, such waves break into ripples whose wavelength depends on λ. This is illustrated in Fig. 3, where the initial overlapping clouds are shown, together with the profile after $t = 10$ ms. For $t < t_s \simeq 9$ ms the shape of the time-evolved cloud is exactly the same for all values of λ. After the shock time t_s, however, the density profile develops a steep density gradient at the cloud boundaries, visible in the figure, which eventually breaks into a train of ripples. The three images shown in Fig. 3 are taken just after the ripples have been produced.

These ripples are characterized by a well-defined wavelength l, which we estimated from the computed profiles. We plot in Fig. 4 the calculated ripple wavelength l as a function of λ. We note that the calculated values for l follows very closely a $\sqrt{\lambda}$ law, which is expected on the basis of dimensional analysis by balancing the energy associated with dispersion to that of the nonlinearity.

In conclusion, we have numerically studied the long-time dynamics of shock waves in the ultracold unitary Fermi gas. We have described the system by using an extended density functional approach, which has been used recently to successfully describe a number of static and dynamical properties of cold Fermi gases. Two main results emerge from our calculations: (a) At zero temperature the simplest regularization process of the shock is purely dispersive, mediated by the quantum gradient term, which is one of the ingredients in our DF approach; (b) the quantum gradient term plays an important role not only in determining the static density profile of small systems, where surface effects are important, but also in the fast dynamics of large systems, where large density gradients may arise.

Finally, we stress that dispersive shock waves with a characteristic wavelength should be observable, according to our simulations, by using a soft-collision setup.

We thank James Joseph and John E. Thomas for useful comments and suggestions, and for having sent us their experimental data.

[1] "The Many-Body X Challenge Problem," formulated by G. F. Bertsch, see R. A. Bishop, Int. J. Mod. Phys. B **15**, 10, iii (2001).

[2] C. Cao, E. Elliott, J. Joseph, H. Wu, J. Petricka, T. Schafer, and J. E. Thomas, Science **331**, 58 (2011).

[3] D. T. Son, Phys. Rev. Lett. **98**, 020604 (2007).

[4] Whereas mass flow in unitary Fermi gas is essentially frictionless, the opposite is true for spin flow, where maximum resistance to flow is observed [5]. As a consequence two clouds of ultracold fermions prepared in different spin states bounce off each other, in spite of the fact that the underlying atomic interaction is attractive and the equilibrium ground state is known to be a paired superfluid.

[5] A. Sommer, M. Ku, G. Roati, and M. W. Zwierlein, Nature (London) **472**, 201 (2011).

[6] L. D. Landau and E. M. Lifshitz, *Fluid Mechanics* (Pergamon, London, 1987).

[7] G. G. Whitham, *Linear and Nonlinear Waves* (Wiley, New York, 1974).

[8] J. A. Joseph, J. E. Thomas, M. Kulkarni, and A. G. Abanov, Phys. Rev. Lett. **106**, 150401 (2011).

[9] J. J. Chang, P. Engels, and M. A. Hoefer, Phys. Rev. Lett. **101**, 170404 (2008); M. A. Hoefer, P. Engels, and J. J. Chang, Physica D **238**, 1311 (2009).

[10] Examples of dispersive shock waves may be found for BEC: Z. Dutton, M. Budde, C. Slowe, and L. V. Hau, Science **293**, 663 (2001); for Fermi gases: E. Bettelheim, A. G. Abanov, and P. Wiegmann, Phys. Rev. Lett. **97**, 246402 (2006); for nonlinear optics: W. Wan, S. Jia, and J. W. Fleischer, Nat. Phys. **3**, 4651 (2007); N. Ghofraniha, C. Conti, G. Ruocco, and S. Trillo, Phys. Rev. Lett. **99**, 043903 (2007).

[11] A. Bulgac, Y.-L. Luo, and K. J. Roche, Phys. Rev. Lett. **108**, 150401 (2012).

[12] A. Bulgac and Y. Yu, Int. J. Mod. Phys. E **13**, 147 (2004); A. Bulgac, Phys. Rev. A **76**, 040502(R) (2007).

[13] L. Salasnich and F. Toigo, Phys. Rev. A **78**, 053626 (2008); **82**, 059902(E) (2010).

[14] S. K. Adhikari and L. Salasnich, Phys. Rev. A **78**, 043616 (2008); L. Salasnich, Laser Phys. **19**, 642 (2009); S. K. Adhikari and L. Salasnich, New J. Phys. **11**, 023011 (2009).

[15] L. Salasnich, F. Ancilotto, and F. Toigo, Laser Phys. Lett. **7**, 78 (2010).
[16] F. Ancilotto, L. Salasnich, and F. Toigo, Phys. Rev. A **79**, 033627 (2009).
[17] L. Salasnich and F. Toigo, J. Low Temp. Phys. **165**, 239 (2011).
[18] L. Salasnich, Europhys. Lett. **96**, 40007 (2011).
[19] C. F. von Weizsäcker, Zeit. Phys. **96**, 431 (1935).
[20] D. Blume, J. von Stecher, and C. H. Greene, Phys. Rev. Lett. **99**, 233201 (2007); J. von Stecher, C. H. Greene, and D. Blume, Phys. Rev. A **76**, 053613 (2007).
[21] A. Bulgac, J. E. Drut, and P. Magierski, Phys. Rev. Lett. **96**, 090404 (2006); **99**, 120401 (2007); Phys. Rev. A **78**, 023625 (2008).
[22] J. Joseph, B. Clancy, L. Luo, J. Kinast, A. Turlapov, and J. E. Thomas, Phys. Rev. Lett. **98**, 170401 (2007).
[23] S. Giorgini, L. P. Pitaevskii, and S. Stringari, Rev. Mod. Phys. **80**, 1215 (2008).
[24] *Mathematical Methods for Digital Computers*, edited by A. Ralston and H. S. Wilf, Vol. 1 (Wiley, New York, 1960), p. 117.
[25] M. Pi, F. Ancilotto, E. Lipparini, and R. Mayol, Physica E **24**, 297 (2004).